

Research Article

Fatih Balli, Mansoor A. Sultan, Aytekin Ozdemir, and J. Todd Hastings

Supplementary Information for "An Ultrabroadband 3D Achromatic Metalens"

<https://doi.org/10.1515/sample-YYYY-XXXX>

Received Month DD, YYYY; revised Month DD, YYYY; accepted Month DD, YYYY

1 Simulation

Simulations are performed by a finite-difference time domain solver (Lumerical Inc.). We obtain the set of phase modulations for different values of hole depth under the assumption of slowly changing geometrical parameters. A plane wave normal to the bottom layer of the the metalens is used as the light source. A nanohole structure is located on top the fused silica substrate and phase modulation is measured using the s-parameters from the field and power monitor. We use periodic and perfectly matching layer boundary conditions (PML) for the transverse and longitudinal directions, respectively. Refractive index, n , of IP-Dip photoresist (Nanoscribe GmbH) is obtained by the Cauchy's equation to model ($n = 1.566 @ 450 \text{ nm}$) [1].

When simulating the entire metalens, we use a total field-scattered field (TFSF) source which is normal to the metalens surface. We simulate only the one quarter of the structure by taking advantage of the symmetry. Anti-symmetric and symmetric boundary conditions are chosen for x-min and y-min boundaries while maximums are set to PML so that simulation time and memory requirements are decreased in an amount 1/4 of the full simulation. The wavelength range of interest was set as 450-1750 μm . We set pulse length, offset and bandwidth 6.6 fs, 19 fs and 133 THz, respectively. A non-uniform mesh was used and the element sizes were automatically determined the by the software. The mesh accuracy was chosen as a compromise between accuracy, memory requirements and simulation time.

The ray tracing algorithm only converges within a certain range of focal lengths for a given EPD. For example, a 20 μm EPD metalens can provide a minimum focal length 208 μm based on recursive ray tracing alone. The corresponding phase derivative at $r = 0$ yields $\phi'_o = 0.56 \text{ rad}/\mu\text{m}$ as shown if Fig. 1-f in the main text. Longer focal lengths are accessible by choosing lower ϕ'_o values. The target phase shifts of TE1 and TE2 are achieved by the nanohole and phase plate (PP) structures, respectively. However, the maximum phase shift through the nanoholes is limited to 4.1 rad. The remaining target phase requirement of TE1 is achieved by thickening the phase plate structure of TE2 under the nanohole so that 0 to 2π phase shift requirement is satisfied. On the other hand, a microlens structure having $f = 45 \mu\text{m}$ and $\text{EPD} = 20 \mu\text{m}$ has a maximum thickness of 1.94 μm at the optical axis as shown in Fig. 1b. Summing the contribution from all three layers results in a minimum and maximum thickness values as 0.47 and 2.74 μm at the radial coordinates $r=0$ and 10 μm , respectively. We can subtract the minimum thickness from the total PP profile since the it does not contribute the total power of the system. Our simulation results reveals that no degradation on the performance is observed after the elimination of the constant thickness layer. Therefore, total thickness of the metalens is reduced from 2.98 to 2.51 μm at $r=0.8 \mu\text{m}$. Total structure provides an average focal length 36 μm . We observe that the power of the total structure is equal to individual contributions coming from the microlens and the metastructure.

Fatih Balli, Physics and Astronomy, University of Kentucky, Lexington, KY 40506, USA

Mansoor A. Sultan, Electrical and Computer Engineering, University of Kentucky, Lexington, KY 40506, USA

Aytekin Ozdemir, College of Optical Sciences, University of Arizona, Tucson, AZ 85721, USA

, Corresponding author: todd.hastings@uky.edu

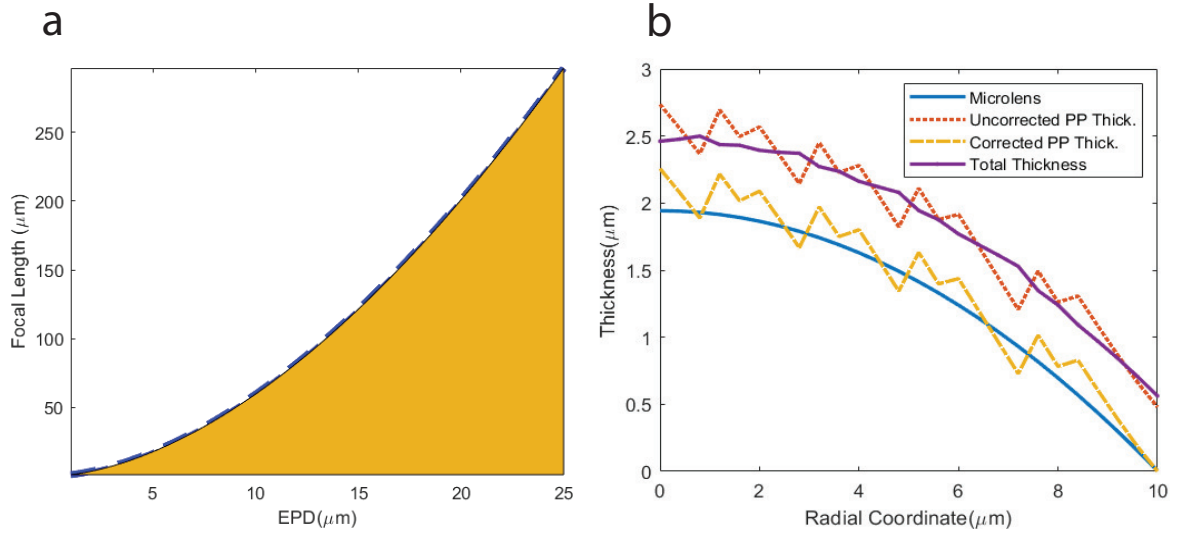


Fig. 1: Focal length limitations and thickness of the metalens. **a** Accessible (white region) and inaccessible (orange region) metalens designs as a function of entrance pupil diameter (EPD) and focal length. Adding an additional microlens structure with a hyperbolic thickness profile allows access to designs in the otherwise inaccessible region while still maintaining achromatic performance. **b** Thickness of the metalens as the function of radial coordinate. Blue curve represents the thickness trend of an isolated microlens with design parameters $f=45 \mu\text{m}$ and $\text{EPD} = 20 \mu\text{m}$. Dashed red and yellow curves are total phase plate thickness values pre and post thickness reduction procedure, respectively. The total thickness trend of the metalens, including the nanohole structures, is represented by the purple curve.

2 Fabrication

The achromatic metalens was fabricated using a Nanoscribe Photonic Professional GT and IP-Dip photoresist (Nanoscribe GmbH, Germany) with a $63\times$ objective in dip-in mode. The structure was processed as an STL file. The hatching and slicing distance for the phase plate was set to 50 nm. The optimal laser power for phase plate writing was 17 mW. After exposure, the sample was developed with 2-Methoxy-1-methylethyl acetate (PGMEA) (Avantor Performance Materials, LLC.) for 45 minutes to remove the unpolymerized resin. The sample was directly immersed in isopropyl alcohol (Fisher Scientific) for 4 minutes to remove the developer (PGMEA), and immediately immersed in lower surface tension fluid for 30 seconds (3M Novec 7100 Engineered Fluid) to protect the structures from deformation when they dry.

Selection of nanoholes compared to pillar structure is based on three distinct advantages that we observed during fabrication process: First, nanopillars provide subwavelength period with durable structures. However, we observe bending of the nanopillars for periods below 750 nm, which prevents us from reaching subwavelength unit cell structures. Second, we observe slight bridging of the photoresist between some pillars. Bending problems become more dominant as we decrease the period. Third, we were able to decrease the fabrication process time. For the hole design, we use a single STL file to process the whole structure. Nanopillars, on the other hand, were typically written using piezo mode which requires the system to print each pillar separately leading to longer fabrication process.

The size of the metalenses is limited by the objective used in our two-photon lithography system. Specifically, the effective printing area is defined by a $200 \mu\text{m}$ diameter circle. The printing quality degrades due to spherical aberration for sizes larger than $200 \mu\text{m}$. Splitting the printing area into fields and stitching them together could yield larger structures. However, field edges cause optical power loss and create disturbing aperture effects around the focal point. Fabrication of millimeter size lenses would be possible even with the current hardware if the efficiency degradation and focus quality is sacrificed. Of course, improvement of the instrumentation to reduce stitching errors would be the preferred route for improvement.

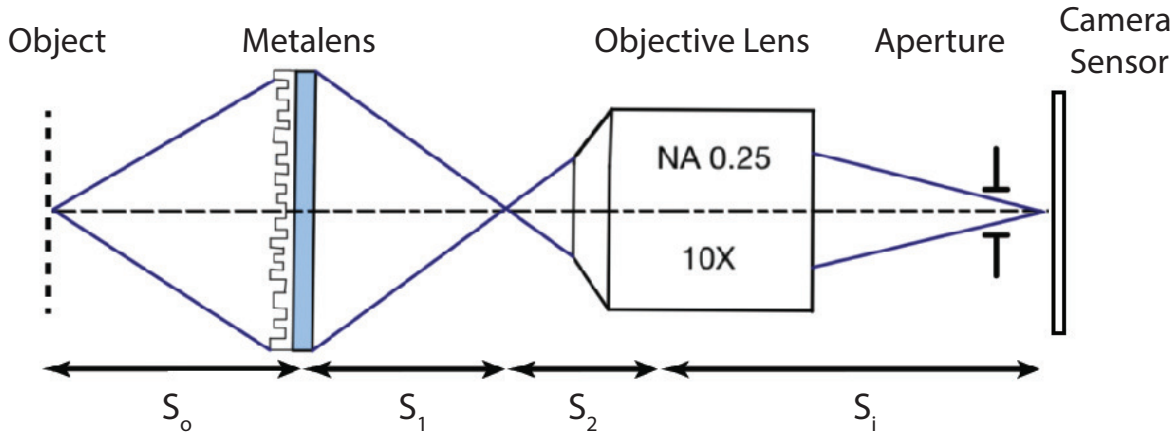


Fig. 2: Optical test setup for imaging with EPD=200 μm , NA=0.04 metalens. Object to metalens distance, S_o , is chosen as 30 mm. An internal image is formed at a distance S_1 from the metalens. We keep the distance between the internal image and the objective, S_2 , variable so that desired magnification is obtained for any object size. The internal image is relayed to a distance S_i from the objective. We use an aperture stop between objective and the camera sensor so the noise is minimized.

The another factor limiting the size of the metalens is the ray tracing method explained in the main text. As we increase the diameter of the metalens, maximum accessible NA value decreases as shown in Fig. 3c in reference [2]. Further improvement of NA for a fixed diameter is possible by adding an air gap between the optical elements. However, this extra separation introduces other trade-offs in efficiency and fabrication difficulty.

3 Optical Testing and Imaging

We use a filtered supercontinuum source (SuperK EXTREME EXW-6 from NKT Photonics) for illumination. We obtain two sets of bandwidths (450 – 850 nm and 1150 – 1800 nm) using an acousto-optic filter (SuperK Select). Discrete wavelengths of 1000 and 1100 nm were obtained by combining a long-pass filter (SuperK Split) and bandpass filters (Thorlabs FB1000-10 & FB1100-10). The optical setup is precisely aligned so that on-axis collimated beam was incident on the metalens surface. The focused beam is again collimated by a 40x objective (Nikon M Plan 40 NA 0.55) and imaged by a tube lens (Mitutoyo MT-1) on a broadband (visible to near infrared) camera (NINOX-VS-CL-640 from Raptor Photonics). Transverse motion along the optical axis is obtained by a motorized stage (Thorlabs MTS25-Z8) in increments of 2 and 0.5 for power intensity and focal error measurements, respectively. Operating bandwidth of the objective does not cover NIR regime, which introduces chromatic aberrations additional to metalens itself. The measure of additional aberration due to optical test setup is determined by imaging a pinhole while sweeping the wavelength from 650-1750 nm. The true focal point for a specific wavelength is determined by comparing diffraction-limited Airy pattern and pin hole image. We determine the focusing efficiency as the ratio of the integrated power within the circle centered at on-axis focal point and having radius $1.5 \times \text{FWHM}$ to the total power incident on the metalens.

For imaging, we use a tungsten-halogen lamp to illuminate the target objects. Illumination at the target wavelength is obtained by band pass filters (Thorlabs FBX-10 series). NIR illumination is obtained by filtering through long-pass filter (Thorlabs FEL1000). The image formed by the metalens is relayed by a 10x objective (Newport M-10X 0.25). Under the thin lens approximation, inverse magnification of the system is given as $M^{-1} = 1 + S_1 \Phi$ where Φ and S_1 are total power of the system and object distance to the metalens. We choose the object space distance as $S_o \sim 30$ mm. We keep the objective location variable

so that suitable magnifications are obtained for different object sizes. Images under full spectrum and NIR illumination are captured by the broadband camera (NINOX-VS-CL-640). The camera's quantum efficiency is relatively flat between 1000 nm and 1650 nm and falls off sharply towards 1700 nm. Thus the camera response sets an effective long wavelength limit. We use a color microscope camera (Amscope MU1000) to capture RGB colored images.

References

- [1] T. Gissibl, S. Wagner, J. Sykora, M. Schmid, and H. Giessen, Refractive index measurements of photo-resists for three-dimensional direct laser writing, *Optical Materials Express* **7**, 2293–2298 (2017).
- [2] F. Balli, M. Sultan, S. K. Lami, and J. T. Hastings, *Nature Communications* **11**, 1 (2020).